4D printing of reconfigurable metamaterials and devices

van Manen, T.; Janbaz, S.; Jansen, K.M.B.; Zadpoor, A.A.

Important note
To cite this publication, please use the final published version (if applicable).
Please check the document version above.

ARTICLE

Check for updates

4D printing of reconfigurable metamaterials and devices

Teunis van Manen [1✉], Shahram Janbaz[1,2], Kaspar M. B. Jansen[3] & Amir A. Zadpoor[1]

Shape-shifting materials are a powerful tool for the fabrication of reconfigurable materials. Upon activation, not only a change in their shape but also a large shift in their material properties can be realized. As compared with the 4D printing of 2D-to-3D shape-shifting materials, the 4D printing of reconfigurable (i.e., 3D-to-3D shape-shifting) materials remains challenging. That is caused by the intrinsically 2D nature of the layer-by-layer manner of fabrication, which limits the possible shape-shifting modes of 4D printed reconfigurable materials. Here, we present a single-step production method for the fabrication and programming of 3D-to-3D shape-changing materials, which requires nothing more than a simple modification of widely available fused deposition modeling (FDM) printers. This simple modification allows the printer to print on curved surfaces. We demonstrate how this modified printer can be combined with various design strategies to achieve high levels of complexity and versatility in the 3D-to-3D shape-shifting behavior of our reconfigurable materials and devices. We showcase the potential of the proposed approach for the fabrication of deployable medical devices including deployable bifurcation stents that are otherwise extremely challenging to create.

[1] Additive Manufacturing Laboratory, Department of Biomechanical Engineering, Delft University of Technology (TU Delft), Delft, The Netherlands. [2] Institute of Physics, University of Amsterdam, Amsterdam, The Netherlands. [3] Emerging Materials Laboratory, Department of Design Engineering, Delft University of Technology (TU Delft), Delft, The Netherlands. ✉email: t.vanmanen@tudelft.nl

Shape-shifting empowers the development of designer materials with advanced functionalities and properties. For example, a flat mechanism can shift its shape into a fully functional robot[1,2]. Other examples are origami-based metamaterials[3–5] or self-folding bio-scaffolds made from (nano-) patterned 2D sheets[6]. There are two major categories of shape-shifting: 2D-to-3D and 3D-to-3D. 2D-to-3D shape-shifting enables flat constructs to fold themselves into geometrically complex 3D objects. The main advantage lies in the ability to employ planar fabrication techniques for affording an ultimately 3D object with functionalities that originate from micro-/nanoscale surface features[7–9]. 3D-to-3D shape-shifting, on the other hand, is particularly useful for the fabrication of reconfigurable materials[10,11]. The 3D configuration of such materials changes upon activation, thereby altering their functions and properties (e.g., stiffness or wave propagation properties[12,13]).

Several strategies for the fabrication of shape-shifting structures are reported in the literature. The vast majority of the existing techniques rely on the use of active materials that change their dimensions upon activation[14–16]. Examples include the swelling of hydrogels submerged in water[17] and the shrinkage of pre-strained shape-memory polymers exposed to high temperatures[18,19]. 4D printing allows for the single-step manufacturing of complex shape-shifting structures[20–22]. The simplest type of 4D printing relies on the introduction of some sort of anisotropy in the material during the printing process[23–27]. Recently, we demonstrated how hobbyist FDM 3D printers and widely available, inexpensive materials can be used to program complex shape-shifting behaviors[26]. This approach, which has received much attention since and makes 4D printing accessible to a wide range of users, is cost-effective, highly scalable, and applicable to many materials.

The main working principle is the introduction of a rationally designed pattern of spatially varying anisotropies into the material. Such a pattern of anisotropy together with the memory stored in the extruded deposited filaments makes it possible to program complex 2D-to-3D shape-shifting behaviors into the fabric of the 4D printed object. The memory stored in the printed polymers (e.g., polylactic acid (PLA) filaments) is a result of simultaneous extrusion during the printing process and the rapid cooling of the extruded filaments under the physical constraints imposed by the neighboring filaments[26]. When heated above their glass transition temperature (T_g), each deposited filament shrinks along its longitudinal direction while expanding in the other directions. The combined, concerted actions of all anisotropically deposited filaments lead to the desired shape-shifting behavior.

While highly effective for 2D-to-3D shape-shifting, our previously proposed approach, as well as similar approaches proposed by others[28,29], are seriously limited by the in-plane nature of their introduced anisotropies, which makes it very challenging to create reconfigurable materials. Here, we circumvent this limitation by printing otherwise planar structures on curved surfaces. We present a simple design of an add-on device, which makes it possible for hobbyist 3D printers to 4D-print on curved surfaces. We use computational models to simulate the shape-shifting behavior of the printed structures and to better understand the underlying mechanisms. Moreover, we demonstrate the potential of our proposed approach through the design and fabrication of various types of reconfigurable materials and devices, including a number of deployable cardiovascular stents.

Results and discussion

Basic shape-shifting elements. We designed and fabricated a simple add-on device, which was then mounted on an inexpensive hobbyist 3D printer (Supplementary Fig. 1). The add-on device employs a stepper motor to rotate a drum on which the specimens are printed. Combined with the three degrees-of-freedom offered by the linear motion system of the 3D printer, the rotating drums allow for the deformation patterns to be programmed along with both longitudinal and circumferential directions. This new concept for the fabrication of curved 3D-to-3D shape-shifting structures is schematically illustrated in Fig. 1a. More details can be found in Supplementary Note 1. Supplementary Video 1 shows the fabrication of a shape-shifting specimen.

To demonstrate the utility of the proposed approach, we used PLA filaments. First, we studied the material properties and deformation characteristics of basic shape-shifting elements. The thermomechanical properties of the PLA filaments were characterized using dynamic mechanical analysis (DMA). Molded PLA specimens were used in order to study the material properties independent from the 3D printing process. The DMA test results reveal a T_g of 70 °C while a clear drop in the mechanical properties upon heating above T_g can be observed (Fig. 1b). Based on the experimental data, a temperature-dependent viscoelastic material model was fitted to be used for finite element analysis (FEA). The model parameters are listed in Supplementary Tables 1, 2, and 4. More methodological details can be found in Supplementary Note 2.

We then studied the shape transformation of individually printed filaments as a function of the printing parameters. Both the layer thickness and extrusion temperature were varied to find the optimal combination of printing parameters. A lower printing temperature and, to a lesser extent, a smaller layer thickness was found to result in an increased filament shrinkage (Fig. 1c and Supplementary Fig. 3a). An extrusion temperature of 180 °C was selected as the lower bound, because PLA filaments do not fully melt below this temperature, rendering the extrusion process very challenging, especially for very thin and very thick layers. The effectively programmed deformation of printed constructs is the combined effect of the introduced molecular orientation along the direction of printing and the cooling history of the material. The molecular orientation is dependent on several factors, such as the molecular alignment introduced within the nozzle and the additional straining caused by the velocity differences between the print-head and rotating shaft. Only the accumulated results of the printing parameters were studied here. These results were, however, consistent between the prints performed on a flatbed and those carried out using a rotating shaft. Reheating and subsequent cooling of the PLA filaments may cause additional relaxation, thereby limiting the magnitude of the programmed deformation. We, therefore, studied the effects of the printing path too. Only for parallel filaments with lengths less than 5 mm, a significant effect of the printing path on the shape-shifting behavior was observed (Fig. 1d and Supplementary Fig. 3b, c). Curves were fit to the experimental data to serve as input to the finite element analysis (FEA) calculations that were performed to describe the shape-shifting behavior of the reconfigurable materials and devices studies here (Supplementary Table 3). More methodological details can be found in Supplementary Note 3.

Based on the knowledge gained regarding the effects of the printing parameters and printing path on the programmed deformations, basic bending elements were designed. The smallest possible in-plane bending element consists of one shrinking line parallel to an expanding block wave pattern (Fig. 1e). Upon increasing the width of the expanding block-wave, the expansion ratio of the elements increases but at the cost of an increase in the bending stiffness. The maximum curvature was found for bending elements with a width of 0.5 mm. Out-of-plane bending elements were fabricated by printing parallel filaments in the longitudinal direction on top of layers with parallel filaments in the transverse direction (Fig. 1f). Again, the degree of the
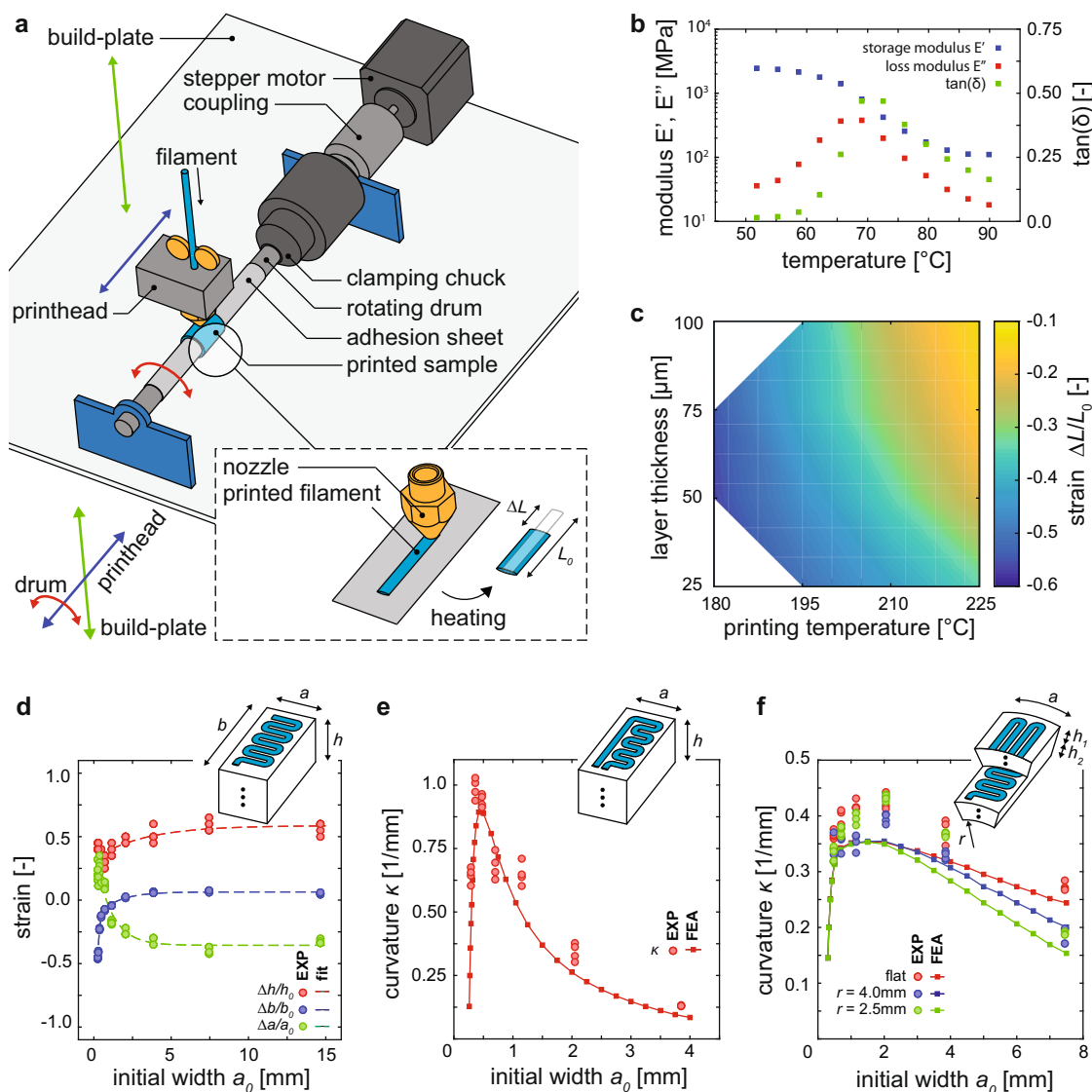
Fig. 1 4D printing concept. a A schematic illustration of the methodology used for the fabrication of curved shape-shifting specimens. **b** The storage modulus, loss modulus, and tan(δ) of the molded PLA specimens for a frequency of 10 Hz. **c** The effects of the layer thickness and printing temperature on the longitudinal shrinkage of the printed filaments. **d–f** The deformation characteristics of the basic building blocks as a function of the initial width. See Supplementary Video 1.

longitudinal expansion of the bottom layers increases for larger widths (a) of the out-of-plane bending elements. However, the increased difference in the longitudinal expansion between the top and bottom layers is accompanied by an opposite difference in the transverse expansion. As the width of the element increases, the bending due to the transverse expansion becomes more dominant, thereby increasing the second moment of inertia in the longitudinal direction. This effect is larger for the specimens with a smaller initial radius of curvature (Fig. 1f). Regardless of the initial curvature, however, the maximum curvature was achieved for a width of 2.0 mm (Fig. 1f). Both for the in-plane and out-of-plane bending elements, FEA was performed in which dimensional changes were calculated with the aid of empirical deformation curves (Fig. 1d). In general, a good agreement between the experiments and FEA simulations was found (Fig. 1e, f). The discrepancies between the experiments and the FEA results may be attributed to the manufacturing imperfections, such as the porosity of the 3D printed specimens, that are not implemented in the computational model. Such porosities may introduce anisotropies in the stiffness of the

bending elements while also affecting the amount of (transverse) expansion[26,30–33]. As a result, the bending stiffness of the elements reduces, resulting in an underestimation of the bending curvature in the computational models. More details on the FEA results can be found in Supplementary Note 4.

Reconfigurable materials. The next step is to apply the developed approach and the basic elements presented above for the design and fabrication of more complex reconfigurable structures. We employed three different design strategies to fabricate a variety of curved shape-changing specimens (Fig. 2). The first strategy is based on introducing spatial variations in the orientation of the printing path along with the circumferential or longitudinal directions, which was used to create multiple sample objects with out-of-plane shape-shifting behaviors caused by buckling (Fig. 2a–c). Using this approach, both the bending of a cylinder, as well as various other types of shape transformations can be programmed in the structure of the material. The second shape-shifting strategy relies on the positioning of in-plane
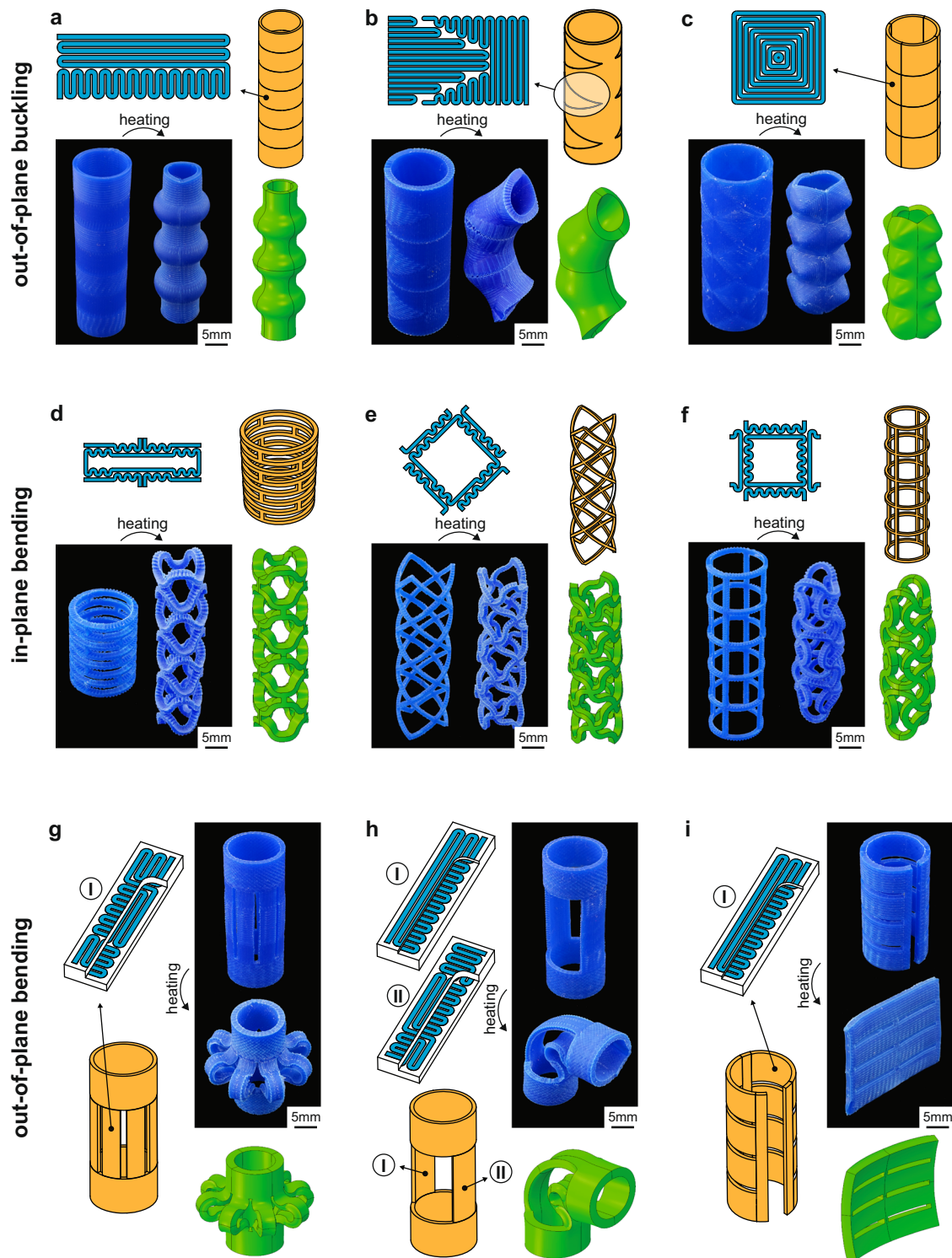
Fig. 2 Shape-shifting of a variety of curved samples. a–c Three examples of out-of-plane buckling specimens employing in-plane deformation patterns. **d–f** The shape-shifting behavior of cylindrical lattices with in-plane bending elements. **g–i** The shape-shifting specimens made of different arrangements of out-of-plane bending elements. In all cases, experimental and computational results are presented side by side. See Supplementary Videos 2–4.

bending elements within lattice structures. Three different types of unit cells were designed, resulting in a variety of shape deformations (Fig. 2d–f). Finally, multiple arrangements of out-of-plane elements connected by semi-passive cylinders (i.e., elements displaying limited amounts of deformation upon activation) were used for the manufacturing of the third series of shape-shifting tubes (Fig. 2g–i). Tubes that shrink along their

longitudinal direction (Fig. 2g), bend (Fig. 2h), or unfold (Fig. 2i) were fabricated. For all the designed specimens, there is a good agreement between the experiments and the FEA results, indicating the effectiveness of the FEA models in predicting the shape-shifting behavior of our 4D printed curved specimens. Supplementary Videos 2–4 show the shape-shifting patterns, as well as the FEA results of the samples presented in Fig. 2.
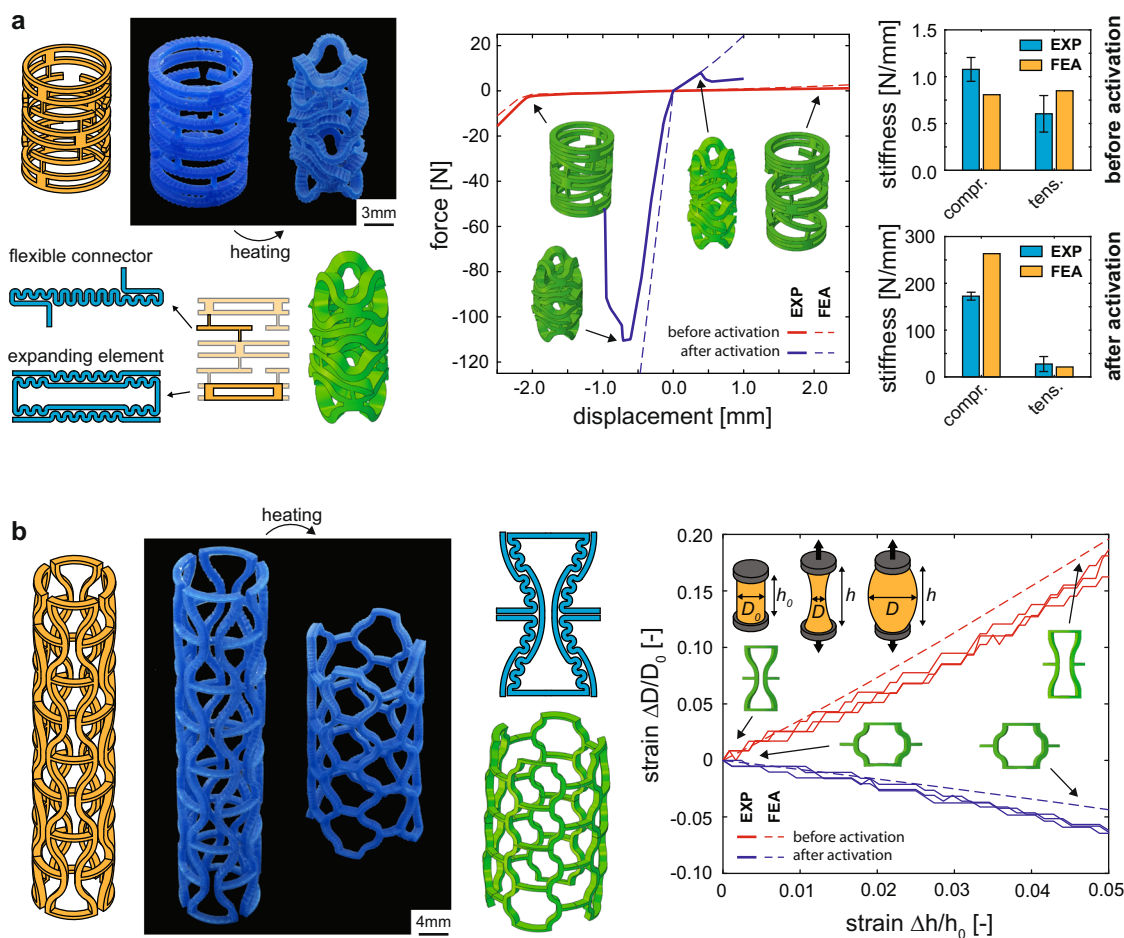
Fig. 3 Switching of mechanical properties. a Shape-shifting structures that switch their mechanical behavior from highly compliant to semi-rigid upon activation. The error bars represent the standard deviation ($n = 3$ per group). **b** The switching of the Poisson's ratio of a 4D printed specimen made using re-entrant unit cells. Upon activation, the specimen switches its mechanical behavior from conventional (i.e., a positive value of the Poisson's ratio) to auxetic (i.e., a negative value of the Poisson's ratio). In all cases, experimental and computational results are presented side by side. See Supplementary Video 5.

Adaptive materials. The method we present here for the fabri-cation of reconfigurable materials, which requires nothing more than a simple modification of widely available FDM 3D printers and inexpensive PLA filaments paves the way for different types of potential applications. Here, we highlight two classes of potential applications, including adaptive materials (i.e., adaptive stiffness and Poisson's ratio) and deployable (medical) devices.

A rational design of the shape-shifting behavior can be used to change specific properties of a material, including its stiffness and Poisson's ratio. We present two such designs. The first design is a compliant structure made of stiff rings connected by flexible elements (Fig. 3a). When subjected to tensile, compressive, twisting, or shearing loads, the dominant deformation mode is the bending of the thin flexures. The stiffness of the specimens, therefore, does not exceed $\approx 1.0 \, \mathrm{N \, mm^{-1}}$ (Fig. 3a). Upon activation, the flexible connectors and expanding rings come into contact with each other. Once those contacts are established, the dominant deformation mode switches to the stretching of the flexures combined with the compression of the stiff rings (Fig. 3a). This programmed change in the deformation regimen results in a shift from a highly compliant structure to a semi-rigid one. In the case of tensile loading, a 30-fold increase in the stiffness is achieved while the compressive stiffness increases even more, by more than 2 orders of magnitude (Fig. 3a). The computational models developed using the material character-istics and shape-memory behavior of simple configurations (Fig. 1) are capable of capturing the constitutive response, as well as the

shape-shifting behavior of the adaptive-stiffness specimens designed here (Fig. 3a). The relatively small differences between the experiments and FEA can be attributed to the local failure of the specimens, which is not included in the FEA models. The second design of adaptive materials presented here consists of a regular assembly of re-entrant honeycomb unit cells (Fig. 3b). The bending of the arms, upon activation, results in switching from a re-entrant unit cell (with auxetic behavior) to conventional honeycomb unit cells (with positive values of the Poisson's ratio) (Fig. 3b). We conducted experiments in which the specimens were subjected to tensile loading both before and after the activation of the shape-shifting behavior. The change in the diameter as a function of the applied stretch is plotted in Fig. 3b. A switch from a negative to a positive Poisson's ratio can, indeed, be observed in these results. This shift in the Poisson's ratio was also captured by our computational model (Fig. 3b). While we only demonstrated two examples of adaptive mechanical behavior, many other types of adaptive behavior are possible. Examples include opposite switching behaviors (i.e., from stiff to compliant or from conventional to auxetic) as well as the switching of other structural properties. Supplementary Video 5 shows the activation of the samples presented in Fig. 3.

Deployable devices. Deployable devices are another interesting area of potential application for the approach presented here.
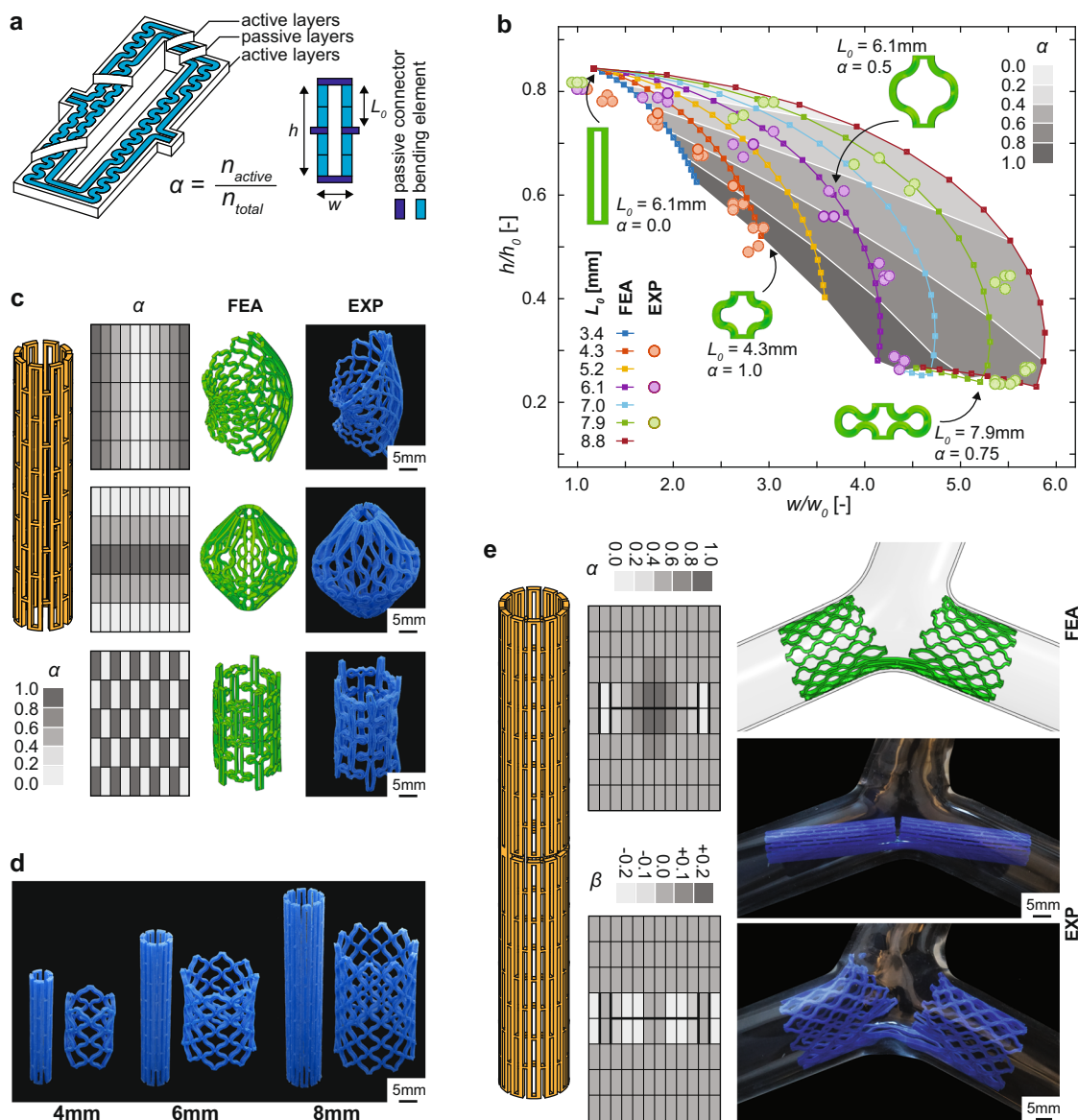
Fig. 4 Deployable materials and devices. a An illustration of the design strategy and printing path of a shape-shifting unit cell made of in-plane bending elements and passive connectors. **b** Computationally and experimentally obtained deformation characteristics of the expandable unit-cell. **c** Deployable cylinders made of different combinations of unit cells. **d** The dimensional scaling of the deployable stents. **e** The deployment of a bifurcation stent within a model artery. See Supplementary Videos 6, 7.

Deployable devices can be transported to otherwise inaccessible places (e.g., in the human body). Subsequently, the device is deployed to fulfill its desired function. Here, we use a specific design of the unit cell to program the shape-shifting behavior of a large variety of deployable structures. The unit cell consists of in-plane bending elements that are joined through small connectors (Fig. 4a). In addition to the initial length of the bending arms (L_0), the amount of bending can be programmed by introducing a number of so-called passive layers within the bending arms. The printing paths of both passive and active layers are illustrated in Fig. 4a. As opposed to active layers, passive layers are designed to remain straight upon activation. The competition between the active and passive layers determines the final curvature of the bending elements. Both experiments and finite element simulations were conducted to study the effects of the number of passive layers (described by the parameter α) and L_0 on the in-plane deformation of the unit cell (see Fig. 4b). As α and L_0 increase, the lateral expansion of the unit cell increases at the cost of an

increased longitudinal shrinkage. Upon activation, unit cells with a larger α and L_0 experience some levels of contact between their bending arms, which limits their expansion (Fig. 4b). The results presented in Fig. 4b can be used as a design map to program a large variety of deployable structures. We designed and fabricated three types of deployable cylinders consisting of an array of 5×10 unit cells. Multiple gradients of α were used, resulting in different deployed geometries even though the initial geometry is the same in all cases (Fig. 4c). Supplementary Video 6 shows the deployment of these three samples.

One important application of deployable structures is in the development of medical devices, including cardiovascular stents. Polymeric stents are particularly interesting because of their superior ability to serve as a drug delivery vehicle[34,35]. Moreover, bioresorbable polymers can be used to eliminate some of the risks associated with permanent stents, such as late stent thrombosis[36–38]. Here, we demonstrate the potential of the presented shape-shifting approach to serving as a platform for the

fabrication of self-expandable polymeric stents. Based on the same unit cell design (Fig. 4a), three uniformly expandable stents were fabricated in different sizes (Fig. 4d). Miniaturized stents can be fabricated using rotating rods with smaller diameters. Upon activation, the stents expand into their permanent shape (Fig. 4d). We designed the stents to show an approximately three-fold increase in diameter. Depending on the selected dimensions of the unit cells, smaller or larger amounts of radial expansion can be achieved as well.

As a final demonstration of the versatility of the presented 4D printing approach, a bifurcation stent was designed and fabricated. The design is based on the same expandable unit cell as described above (Fig. 4a). In addition to α, there are two other design features that affect the shape-shifting behavior of unit cells with a length of L_0. First, some of the connections between neighboring unit cells were removed in order to decouple the expansion in the tangential and longitudinal directions. Second, a degree of out-of-plane bending of individual unit cells was introduced by off-center positioning of the passive layers. The amount of the programmed out-of-plane actuation is described by the dimensionless parameter β:

$$\beta = \frac{n_{\text{active,top}} - n_{\text{active,bottom}}}{n_{\text{total}}}$$

where $n_{\text{active,top}}$ is the number of active layers on top of the passive layers while $n_{\text{active,bottom}}$ is the number of active layers underneath the passive layers. The spatial control of α and β, as well as the connections between unit cells, allows for the programming of even more complex shape-shifting patterns. We designed a bifurcation stent by assembling an array of 8×12 unit cells (Fig. 4e). The removed connections are indicated by a thick black line. Upon activation, the bifurcation stent expands and an anchor point for the connection of a side-branch stent opens up. We used a model artery to activate the bifurcation stent and demonstrate its flexibility in morphing the geometry of the artery (Fig. 4e). Supplementary Video 7 shows the activation of both a conventional, as well as a bifurcation stent.

Conclusions

In summary, we presented a method for the fabrication of reconfigurable materials. Commercially available FDM 3D printers were modified through the addition of a simple device that can be easily manufactured in most basic workshops (if not domestic kitchens). By printing the specimens on a rotating shaft, we could incorporate both in-plane and on-curvature anisotropies into the fabric of 4D printed constructs. We then used the proposed approach to demonstrate the high level of geometrical complexity that can be achieved in the 3D-to-3D shape-shifting behavior of reconfigurable materials and devices. We also demonstrated some potential applications of the proposed reconfigurable materials, including those with adaptive effective properties (i.e., adaptive stiffnesses and switchable auxeticity) as well as deployable (medical) devices. While we only used PLA filaments in this study, a wide range of shape memory polymers with highly variable values of the glass transition temperatures can be used for the fabrication of 4D printed devices. Polymers with lower values of the glass transition temperature already exist[39] and can be used in low-temperature applications. The underlying concepts of the approach proposed here remain valid regardless of the material used. While we performed most of our experiments using a hot water bath, not all potential applications are compatible with a liquid activation medium. We, therefore, conducted a number of experiments using hot air as the activation medium to understand the effects of the activation medium on the resulting shape-shifting behavior. The results of our experiments confirmed that the shape-shifting behavior of the specimens fabricated using the presented 4D printing approach is largely independent of the activation medium (Supplementary Fig. 4). In any case, short activation times (typically less than 30 s) were sufficient to complete the shape-shifting process, which is highly beneficial for most practical applications. We believe that the development of such types of low-entry-barrier 4D printing technologies is essential for the democratization of emerging digital fabrication technologies and ensures they remain globally accessible including in low-resource settings.

Methods

Sample fabrication. All the specimens were fabricated from PLA filaments using an FDM 3D printer (Ultimaker 2+, Ultimaker, The Netherlands). The add-on device (Fig. 1a) was designed as a rotating drum mounted on a frame made from laser-cut acrylic sheets. The design and manufacturing details are presented in the supplementary document (Supplementary Tables 5 and 6). Good adhesion between the rotating drum and the printing specimens was guaranteed by the means of adhesion sheets. Both the printing paths and GCode files were generated using custom programs written in MATLAB (Mathworks, US). Supplementary Notes 1, 5, and 7 can be consulted for extensive details on the fabrication process including the specific fabrication parameters for all the specimens presented in this study.

Sample activation. Samples were activated using a transparent container filled with hot water. The temperature was controlled by a heating immersion circulator (CORIO CD, Julabo, Germany). The deformations of the specimens were captured using digital cameras. The specimens were submerged in the water bath with a temperature of 90 °C for at least 30 s to ensure the shape-shifting process was complete (see Supplementary Note 6).

Characterization of the constitutive behavior. The temperature-dependent mechanical properties of PLA were measured by performing dynamic mechanical analysis (DMA) measurements using a TA-Instruments Q-800 machine (TA Instruments, US). Assuming the material to be thermorheologically simple, the time-temperature superposition principle was applied. A master curve was constructed by shifting the measured storage modulus at different temperatures along the frequency axis. The resulting master curve with the corresponding shift factors (a_τ) was then obtained. The Williams-Landel-Ferry (WLF) equation was fit to the experimental results and was used for the further analyses performed here (Supplementary Fig. 2).

Finite element analysis. FEA was performed using the commercial software Abaqus (Abaqus 6.14, Simulia, US). A transient coupled temperature-displacement analysis was performed (Abaqus Standard, nonlinear implicit solver, full Newton integration) in order to also capture the time-dependent material behavior. The geometries of the computational models were discretized using full-integrated solid temperature-displacement elements (i.e., C3D8T in Abaqus). The viscoelastic behavior of PLA was modeled using a Prony series. The simulation time was set to 2 min to ensure the completeness of the shape-shifting process. For some of the models, a surface-to-surface contact definition was implemented to prevent the penetration of different parts of the structure. A penalty contact enforcement algorithm was used for that purpose. The full details of the material characterization using DMA, material models, computational procedures, and the other methodological aspects of the computational modeling approach are presented in Supplementary Notes 2 and 4.

Data availability

The data that support the findings of this study are available from the corresponding author upon reasonable request.

References

1. Felton, S. et al. A method for building self-folding machines. *Science* **345**, 644–646 (2014).
2. Rus, D. & Tolley, M. T. Design, fabrication and control of origami robots. *Nat. Rev. Mater.* **3**, 101–112. (2018).
3. Filipov, E. T., Tachi, T. & Paulino, G. H. Origami tubes assembled into stiff, yet reconfigurable structures and metamaterials. *Proc. Natl Acad. Sci. USA* **112**, 12321–12326 (2015).
4. Overvelde, J. T. et al. Rational design of reconfigurable prismatic architected materials. *Nature* **541**, 347–352 (2017).
5. Ning, X. et al. Assembly of advanced materials into 3D functional structures by methods inspired by origami and kirigami: a review. *Adv. Mater. Interfaces* **5**, 1800284 (2018).

6. Jamal, M. et al. Directed growth of fibroblasts into three dimensional micropatterned geometries via self-assembling scaffolds. *Biomaterials* **31**, 1683–1690 (2010).

7. Cho, J.-H. et al. Nanoscale origami for 3D optics. *Small* **7**, 1943–1948 (2011).

8. Janbaz, S. et al. Origami lattices with free-form surface ornaments. *Sci. Adv.* **3**, eaao1595 (2017).

9. van Manen, T. et al. Kirigami-enabled self-folding origami. *Mater. Today* **32**, 59–67 (2020).

10. Bobbert, F. et al. Russian doll deployable meta-implants: fusion of kirigami, origami, and multi-stability. *Mater. Design* **191**, 108624 (2020).

11. Haghpanah, B. et al. Multistable shape-reconfigurable architected materials. *Adv. Mater.* **28**, 7915–7920 (2016).

12. Overvelde, J. T. et al. A three-dimensional actuated origami-inspired transformable metamaterial with multiple degrees of freedom. *Nat. Commun.* **7**, 1–8 (2016).

13. Yang, C. et al. 4D printing reconfigurable, deployable and mechanically tunable metamaterials. *Mater. Horizons* **6**, 1244–1250 (2019).

14. Liu, Y., Genzer, J. & Dickey, M. D. "2D or not 2D": Shape-programming polymer sheets. *Progress Polymer Sci.* **52**, 79–106 (2016).

15. van Manen, T., Janbaz, S. & Zadpoor, A. A. Programming the shape-shifting of flat soft matter. *Mater. Today* **21**, 144–163 (2018).

16. Zhang, Y. et al. Printing, folding and assembly methods for forming 3D mesostructures in advanced materials. *Nat. Rev. Mater.* **2**, 1–17 (2017).

17. Ionov, L. Polymeric actuators. *Langmuir* **31**, 5015–5024 (2015).

18. Lendlein, A. & Langer, R. Biodegradable, elastic shape-memory polymers for potential biomedical applications. *Science* **296**, 1673–1676 (2002).

19. Zhao, Q., Qi, H. J. & Xie, T. Recent progress in shape memory polymer: New behavior, enabling materials, and mechanistic understanding. *Progress Polymer Sci.* **49**, 79–120 (2015).

20. Ding, Z. et al. Direct 4D printing via active composite materials. *Sci. Adv.* **3**, e1602890 (2017).

21. Raviv, D. et al. Active printed materials for complex self-evolving deformations. *Sci. Rep.* **4**, 7422 (2014).

22. Zhao, Z. et al. Desolvation induced origami of photocurable polymers by digit light processing. *Macromol. Rapid Commun.* **38**, 1600625 (2017).

23. Ambulo, C. P. et al. Four-dimensional printing of liquid crystal elastomers. *ACS Appl. Mater. Interfaces* **9**, 37332–37339 (2017).

24. Gladman, A. S. et al. Biomimetic 4D printing. *Nat. Mater.* **15**, 413–418 (2016).

25. Kotikian, A. et al. 3D printing of liquid crystal elastomeric actuators with spatially programed nematic order. *Adv. Mater.* **30**, 1706164 (2018).

26. van Manen, T., Janbaz, S. & Zadpoor, A. A. Programming 2D/3D shape-shifting with hobbyist 3D printers. *Mater. Horizons* **4**, 1064–1069 (2017).

27. Kim, Y. et al. Printing ferromagnetic domains for untethered fast-transforming soft materials. *Nature* **558**, 274–279 (2018).

28. Lewis, J. A. & Gratson, G. M. Direct writing in three dimensions. *Mater. Today* **7**, 32–39 (2004).

29. Truby, R. L. & Lewis, J. A. Printing soft matter in three dimensions. *Nature* **540**, 371–378 (2016).

30. Song, Y. et al. Measurements of the mechanical response of unidirectional 3D-printed PLA. *Mater. Design* **123**, 154–164 (2017).

31. Liao, Y. et al. Effect of porosity and crystallinity on 3D printed PLA properties. *Polymers* **11**, 1487 (2019).

32. Lubombo, C. & Huneault, M. A. Effect of infill patterns on the mechanical performance of lightweight 3D-printed cellular PLA parts. *Mater. Today Commun.* **17**, 214–228 (2018).

33. Le Duigou, A. et al. 3D printing of wood fibre biocomposites: from mechanical to actuation functionality. *Mater. Design* **96**, 106–114 (2016).

34. Im, S. H., Jung, Y. & Kim, S. H. Current status and future direction of biodegradable metallic and polymeric vascular scaffolds for next-generation stents. *Acta Biomater.* **60**, 3–22 (2017).

35. Peng, T., Gibula, P. & Goosen, M. F. Role of polymers in improving the results of stenting in coronary arteries. *Biomaterials* **17**, 685–694 (1996).

36. Stefanini, G. G. et al. Biodegradable polymer drug-eluting stents reduce the risk of stent thrombosis at 4 years in patients undergoing percutaneous coronary intervention: a pooled analysis of individual patient data from the ISAR-TEST 3, ISAR-TEST 4, and LEADERS randomized trials. *Eur. Heart J.* **33**, 1214–1222 (2012).

37. Ang, H. Y. et al. Bioresorbable stents: current and upcoming bioresorbable technologies. *Int. J. Cardiol.* **228**, 931–939 (2017).

38. Iqbal, J. et al. Bioresorbable scaffolds: rationale, current status, challenges, and future. *Eur. Heart J.* **35**, 765–776 (2014).

39. Meng, Y., Jiang, J. & Anthamatten, M. Body temperature triggered shape-memory polymers with high elastic energy storage capacity. *J. Polymer Sci. Part B* **54**, 1397–1404 (2016).

Acknowledgements

Author contributions

T.M. and A.A.Z. conceived the study. T.M. designed and fabricated the specimens, conducted the experiments, and performed the computational analysis. T.M. and K.M.B.J. performed the DMA analysis and developed the material model. S.J. assisted with data interpretation and manuscript preparation. T.M. and A.A.Z. wrote the manuscript. A.A.Z. supervised the project. All authors contributed to the analysis of the results, the reading and editing of the manuscript, and the approval of the final version.

Competing interests

The authors declare no competing interests.

Additional information

Supplementary information The online version contains supplementary material available at https://doi.org/10.1038/s43246-021-00165-8.

Correspondence and requests for materials should be addressed to T.v.M.

Peer review information *Communications Materials* thanks the anonymous reviewers for their contribution to the peer review of this work. Primary handling editor: Aldo Isidori. Peer reviewer reports are available.

Reprints and permission information is available at http://www.nature.com/reprints

Publisher's note Springer Nature remains neutral with regard to jurisdictional claims in published maps and institutional affiliations.